The Astrophysical Journal Letters, 905:L28 (7pp), 2020 December 20 https://doi.org/10.3847/2041-8213/abcaf5

Dark Sirens to Resolve the Hubble–Lemaître Tension

Ssohrab Borhanian[1], Arnab Dhani[1], Anuradha Gupta[2], K. G. Arun[3], and B. S. Sathyaprakash[1,4,5]
[1] Institute for Gravitation and the Cosmos, Department of Physics, Pennsylvania State University, University Park, PA 16802, USA; sub284@psu.edu
[2] Department of Physics and Astronomy, The University of Mississippi, Oxford, MS 38677, USA
[3] Chennai Mathematical Institute, Siruseri, 603103, India
[4] Department of Astronomy & Astrophysics, Pennsylvania State University, University Park, PA 16802, USA
[5] School of Physics and Astronomy, Cardiff University, Cardiff CF24 3AA, UK
Received 2020 October 8; accepted 2020 November 14; published 2020 December 21

Abstract

The planned sensitivity upgrades to the LIGO and Virgo facilities could uniquely identify host galaxies of *dark sirens*—compact binary coalescences without any electromagnetic counterparts—within a redshift of $z = 0.1$. This is aided by the higher-order spherical harmonic modes present in the gravitational-wave signal, which also improve distance estimation. In conjunction, sensitivity upgrades and higher modes will facilitate an accurate, independent measurement of the host galaxy's redshift in addition to the luminosity distance from the gravitational-wave observation to infer the Hubble–Lemaître constant H_0 to better than a few percent in 5 yr. A possible Voyager upgrade or third-generation facilities would further solidify the role of dark sirens for precision cosmology in the future.

Unified Astronomy Thesaurus concepts: Cosmology (343); Hubble constant (758); Hubble's law (763); Compact binary stars (283); Gravitational wave astronomy (675); Gravitational wave sources (677); Gravitational wave detectors (676)

1. Introduction

The Hubble–Lemaître constant H_0 is a fundamental cosmological quantity that governs the expansion rate of the universe. Measurements of H_0 from different astronomical observations are at odds with each other. For instance, H_0 inferred from the fluctuation spectrum of the cosmic microwave background (Aghanim et al. 2020) disagrees with the value obtained from the measurement of the luminosity distance and redshift to Type Ia supernovae (Freedman et al. 2019; Riess et al. 2019; Wong et al. 2020) at 4.0σ–5.8σ significance (Riess et al. 2019; Verde et al. 2019). Confirming or ruling out this discrepancy is of paramount importance as it may point to new or missing physics from an epoch in the early universe just before the recombination era (Verde et al. 2019).

Gravitational waves (GWs) facilitate a unique way of determining H_0, without relying on the cosmic distance ladder (Schutz 1986; Holz & Hughes 2005). The multi-messenger observations of the binary neutron star merger GW170817 (Abbott et al. 2017b) led to the first GW-assisted measurement of H_0, estimating its value to be $70^{+12}_{-8}\,\mathrm{km\,s^{-1}\,Mpc^{-1}}$ (Abbott et al. 2017a). This measurement crucially relied on the coincident detection of an electromagnetic (EM) counterpart to the GW source. The source's redshift came from the counterpart, while the luminosity distance was inferred from the GW signal. Observation of EM counterparts to ∼50 binary neutron star mergers could nail down the Hubble–Lemaître constant to an accuracy of 2%, sufficient to confirm if there are any systematics in the local measurements of H_0 (Chen et al. 2018).

2. H_0 with Dark Sirens

Binary black hole (BBH) mergers are not expected to have EM counterparts but they too can determine the luminosity distance to their hosts independently of the cosmic distance ladder; for this reason they are sometimes referred to as *dark sirens*. Even so, it may be possible to identify their potential host galaxies either with the help of a galaxy catalog or by follow-up observations (Nishizawa 2017; Yu et al. 2020). There is no guarantee that this approach could identify the true host as the GW sky localization with current generation detectors is not precise enough (Abbott et al. 2018a). With multiple potential hosts one has to resort to a statistical approach to determine H_0 as first suggested in Schutz (1986). Dark sirens detected in the first and second observing runs of LIGO and Virgo (Abbott et al. 2019c) were used in this way to estimate the value of H_0 to be $68^{+14}_{-7}\,\mathrm{km\,s^{-1}\,Mpc^{-1}}$ (Abbott et al. 2019a).

One source of systematic errors in this method arises from the incompleteness of the available galaxy catalogs. Three galaxy catalogs were used in Abbott et al. (2019a): The first one is the GLADE catalog (Dálya et al. 2018), which has an all-sky coverage, but the probability of the host galaxy to be in the catalog at $z = 0.1$, as determined in Abbott et al. (2019a), is ∼60%. The other two catalogs are from the Dark Energy Survey (an ongoing 5 yr survey) (Abbott et al. 2018b; Drlica-Wagner et al. 2018) and GWENS (SDSS 2016), which are mostly complete up to $z = 0.1$, but do not cover the complete sky, with the former covering only an eighth of the sky at the end of its mission. Nonetheless, LIGO and Virgo at their design sensitivity could constrain H_0 with dark sirens to 5% accuracy with ∼250 detections (Gray et al. 2020).

3. Motivation for Current Work

Recently, LIGO and Virgo have published two compact binary mergers found during the third observing run: GW190412 (Abbott et al. 2020a) and GW190814 (Abbott et al. 2020b), which are exceptional due to their large mass-asymmetry, with mass ratios ∼3 and ∼9, respectively. These systems have led to the detection of subdominant spherical harmonic modes beyond the quadrupole mode (Roy et al. 2019;

Abbott et al. 2020a, 2020b). Such higher modes have been argued to be of importance in the parameter estimation of asymmetric binaries (Arun et al. 2007; Van Den Broeck & Sengupta 2007; Graff et al. 2015), especially that of the luminosity distance D_L and orbital inclination ι (Ajith & Bose 2009). Indeed, among all the dark compact binaries detected to date, GW190814 has the best measured luminosity distance ($\sim$18%) and 90% credible sky area ($\sim$19 deg^2) (Abbott et al. 2020b), albeit its signal-to-noise ratio (S/N) is similar to that of GW150914, whose uncertainty in distance is $\sim$35% (Abbott et al. 2019c). The first LIGO–Virgo GW transient catalog GWTC-1 (Abbott et al. 2019c) includes 10 BBHs, of which some are broadly similar to GW150914. Future observations could potentially improve parameter estimations of such systems when higher modes are present in the observed signal.

We show that the recent discoveries have raised the opportunity to measure H_0 with dark sirens to within 2%, the accuracy required to resolve the Hubble tension, in the next 5 yr. There are two principal reasons for this expectation: (1) planned upgrades to LIGO and Virgo would enhance their sensitive volume by a factor of $\sim$3.4, and (2) higher spherical harmonic GW modes, as shown in the Appendix, should help localize dark sirens in the sky by a factor of $\sim$2 better but, more critically, reduce the uncertainty in distance measurement (Ajith & Bose 2009; Kalaghatgi et al. 2020) by a factor as large as 6 for the populations we study below. These improvements compound together to localize a "golden" subset of the dark sirens to a small enough patch in the sky that only a single galaxy would be found within the error region. Galaxy catalogs and EM follow-up campaigns could then determine the host, obtain the source's redshift, and hence directly measure H_0, without relying on the statistical method (Howell et al. 2018; Kuns et al. 2020b).

We are primarily interested in the local measurement of H_0 with sources close enough that we can neglect the effect of weak lensing (Holz & Hughes 2005) as well as dark matter and dark energy and assume the simplest form of the Hubble–Lemaître law. If sources are too close (say, $D_L \lesssim 100$ Mpc), H_0 measurements will be flawed due to the systematic bias from peculiar velocities v_p of host galaxies. While galaxies in clusters have relatively large peculiar velocities ($v_p \sim 2000$ km s^{-1}), this appears not to be the case ($v_p \sim 300$ km s^{-1}) for the majority of galaxies ($\sim$95%) that are found outside of clusters (Bahcall 1995). Therefore, we will consider, in our study, dark sirens distributed uniformly in comoving volume up to a redshift of $z = 0.1$, corresponding to a luminosity distance $D_L \simeq 475$ Mpc for the Planck 2015 cosmology (Ade et al. 2016). This ascertains that most sources are far enough away ($\sim$1% will be closer than $D_L \sim 100$ Mpc) that the Hubble–Lemaître flow will dominate the peculiar velocities.

4. Dark Siren Populations for H_0

We consider three types of dark siren populations in our analysis and compute the precision with which H_0 could be measured with golden binaries among those populations. The first population makes use of the rates and mass distributions inferred from the GWTC-1 BBHs (Abbott et al. 2019b, 2019c). The second population represents the heavy BBH subpopulation of GWTC-1 with companion masses larger than 25 $M_\odot$. The binaries in this population might be among the loudest that GW detectors can observe. Their projected merger rate makes them an interesting target to consider in our study. Finally, we consider a population of GW190814-like dark sirens. The interest in this class of sources stems from the expected role higher modes may play in parameter estimation.

The simulated populations differ in the choice of companion masses, which are all specified in the source frame in this study. In the case of the full GWTC-1 BBH population, we distribute the larger mass $m_1 \in [5\,M_\odot, 100\,M_\odot]$ according to a power law $p(m_1) \propto m_1^{-\alpha}$ with exponent $\alpha = 1.6$ and the smaller mass m_2 uniformly in the range $[5\,M_\odot, m_1]$ (Abbott et al. 2019b). The heavy BBH population only differs by increased lower-mass bounds: $m_1, m_2 \geqslant 25\,M_\odot$. Finally, the component masses are fixed to $m_1 = 23\,M_\odot$ and $m_2 = 2.6\,M_\odot$ for GW190814-like events (Abbott et al. 2020b). In all the cases, the companion black holes are assumed to be nonspinning, consistent with GWTC-1. Further, the events are uniformly distributed in comoving volume, according to Ade et al. (2016), up to redshift $z = 0.1$, as well as over sky positions, and orientation angles. Each simulated population contains 10^4 samples.

We consistently employ the `IMRPhenomHM` (London et al. 2018) model from `lalsimulation` (LIGO Scientific Collaboration 2018) for the parameter estimation of all the aforementioned classes of sources. This waveform family includes radiative moments with spherical harmonic indices $(\ell, m) = (2, 2), (3, 3), (4, 4), (2, 1), (3, 2), (4, 3)$, which ensures that there are no systematic biases due to the neglect of higher modes and helps us carry out meaningful comparisons between the three populations.

The median merger rate for each population reported by LIGO and Virgo is $\mathcal{R}_{\rm GW190814\text{-}like} = 7^{+16}_{-6}\,{\rm Gpc^{-3}\,yr^{-1}}$ for GW190814-like events (Abbott et al. 2020b) and $\mathcal{R}_{\rm GWTC-1} = 53^{+59}_{-20}\,{\rm Gpc^{-3}\,yr^{-1}}$ for GWTC-1 BBHs (Abbott et al. 2019b). Since we restrict the populations to a maximum luminosity distance of $D_L = 475$ Mpc, we obtain the median merger rates in the volume of interest for these populations to be $\bar{\mathcal{R}}_{\rm GW190814\text{-}like} = 3.1\,{\rm yr^{-1}}$ and $\bar{\mathcal{R}}_{\rm GWTC-1} = 24\,{\rm yr^{-1}}$. Consequently, we obtain $\bar{\mathcal{R}}_{\rm heavy} = 2.9\,{\rm yr^{-1}}$ for heavy BBH events, where we assume that $\bar{\mathcal{R}}_{\rm heavy} = f\,\bar{\mathcal{R}}_{\rm GWTC-1}$ and f to be the fraction of GWTC-1 BBHs with $m_1, m_2 \geqslant 25\,M_\odot$:

$$f \simeq 1.9 \int_{25}^{100} dm_1\, m_1^{-1.6} \int_{25}^{m1} dm_2\, \frac{1}{m_1 - 5} \simeq 0.12.$$

These rates will be used below to estimate the number of dark sirens that could be localized well enough each year to identify their hosts.

5. Detector Networks

The detector networks considered in this study are combinations of seven geographical locations and three technology generations (essentially, the choice of detector's power spectral density) as summarized in Table 1. A+, AdV+, and KAGRA+ (LSC 2016; Kuns et al. 2020a) are planned upgrades of the Advanced LIGO (Aasi et al. 2015), Advanced Virgo (Acernese et al. 2015), and KAGRA (Akutsu et al. 2019) detectors, referred to as 2G+. Their targeted strain sensitivity should improve the reach for BBHs by a factor of $\sim$1.5. We consider two 2G+ networks, HLV+ and HLVKI+, with three and five detectors, respectively. The third network, Voy+, is

Table 1
An Overview of the Four Networks Used to Benchmark GW Detections in the Study

Network Label	Detector Location (Technology)
HLV+	Hanford WA (A+), Livingston LA (A+), Cascina Italy (AdV+)
HLVKI+	Hanford WA (A+), Livingston LA (A+), Cascina Italy (AdV+), Kamioka Japan (KAGRA+), Hingoli India (A+)
Voy+	Hanford WA (Voyager), Livingston (Voyager), Cascina Italy (AdV+), Kamioka Japan (KAGRA+), Hingoli India (Voyager)
ECC	Cascina Italy (ET-D), fiducial US site (CE1), fiducial Australian site (CE1)

Note. The location determines the detector antenna patterns and location phase factors, while the technology indicates the used power spectral density. The Voyager and Cosmic Explorer power spectral densities are chosen to be low-frequency optimized and in the case of the latter for a detector arm length of 40 km.

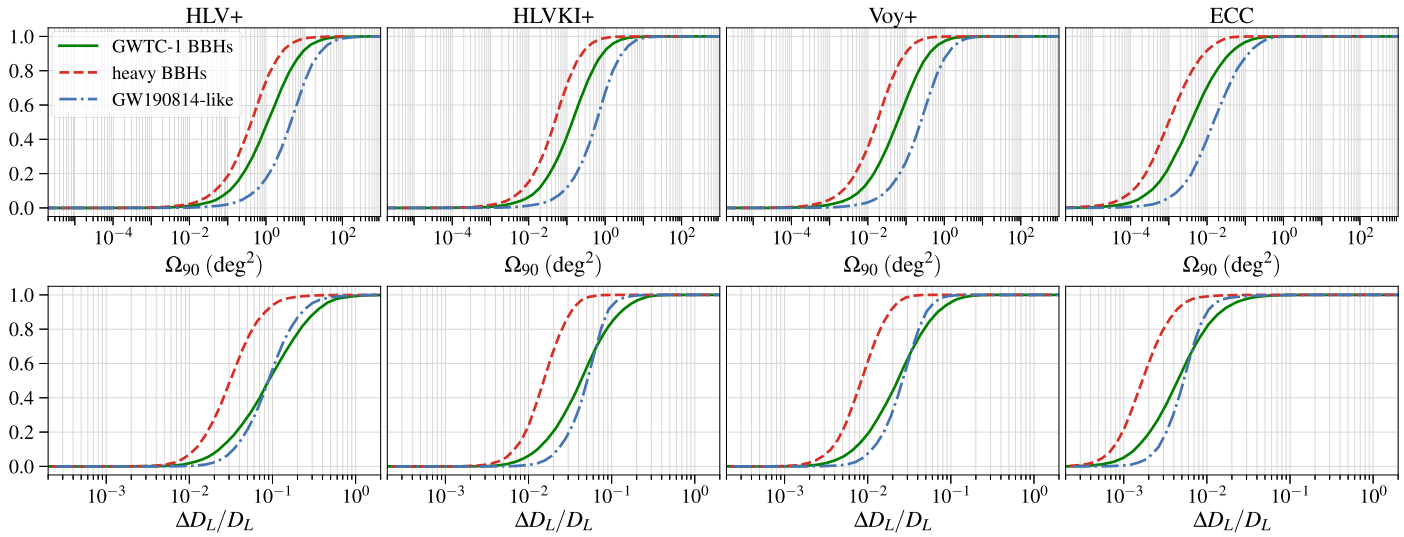

Figure 1. Cumulative density functions of the 90% credible sky area Ω_{90} and fractional luminosity distance error $\Delta D_L/D_L$ for three dark siren populations (GWTC-1 BBHs, heavy BBHs, and GW190814-like) in the four studied networks. The populations contain 10^4 binaries. The crossover in the curves of the GWTC-1 BBH and GW190814-like populations in the lower panels is likely due to the trade-off between measurement accuracies obtained from massive binaries and asymmetric ones.

heterogeneous and uses two 2G+ and three "2.5G" detectors; the latter is a proposed upgrade of the LIGO facilities to "Voyager" technology (Adhikari et al. 2020), which will introduce a further improvement in their reach by a factor of ∼3.2 compared to 2G+. The final network, ECC, contains three third-generation (3G) observatories, namely, one Einstein Telescope (Punturo et al. 2010) in Italy and two Cosmic Explorer detectors (Reitze et al. 2019) at fiducial sites in the United States and Australia. The used power spectral densities, ET-D and CE1 (Kuns et al. 2020a), yield strain sensitivity improvements by factors of ∼3 and ∼5, respectively, as compared to Voyager.

6. Measurement Accuracies

For each of the above networks, we compute numerically the error in the estimation of the binary parameters using the Fisher-matrix formalism (Cutler & Flanagan 1994), which is an excellent approximation for the high-S/N events such as the ones in our three populations. The parameter set includes the binary's intrinsic masses, m_1 and m_2, two angles describing the position of the binary in the sky (R.A. α and decl. δ), two more giving its orientation relative to the detector (inclination ι of the binary's orbital angular momentum relative to the line of sight and the polarization angle ψ), the luminosity distance D_L, a fiducial coalescence time, and the phase of the signal at that time. Among these, D_L and ι are highly correlated when the observed signal is face-on and contains only the $\ell = 2$ quadrupole mode, but the degeneracy is largely lifted by higher-order spherical harmonic modes, $\ell > 2$ (Ajith & Bose 2009; Calderón Bustillo et al. 2020). Gravitational waves from coalescing binaries are dominated by the quadrupole mode; however, higher modes are present in systems with unequal-mass companions and are more prominent for systems observed with large inclination angles.

Figure 1 shows the cumulative density functions of the 90% credible sky area Ω_{90} and fractional luminosity distance error $\Delta D_L/D_L$ for each of the three dark siren populations in the four studied networks. The heavy BBH population allows for better constraints on D_L and Ω_{90} due to the large S/Ns such massive mergers would accumulate. The GW190814-like events will be able to determine the luminosity distance to similar accuracies as GWTC-1 BBHs, but fall behind in terms of the sky localization. The improved parameter estimation, for GW190814-like signals with relatively low S/Ns, is facilitated by the higher modes that are strongly excited for such highly asymmetric systems.

These findings present the two quantities in an "event-independent" fashion. We tackle this by applying a sky localization condition to each event. A sky patch of size $\Omega^* \simeq 4.4 \times 10^{-2}\,\mathrm{deg}^2$ contains, on average, one galaxy with luminosity $L \geqslant L_{10} = 10^{10}\,L_\odot$ within $z = 0.1$ (refer to

Table 2
The Medians of the Signal-to-noise Ratio $\langle\rho\rangle$ and Fractional Error in Luminosity Distance $\langle\Delta D_L/D_L\rangle$ for Three Dark Siren Populations, GWTC-1 BBHs, Heavy BBHs, and GW190814-like

Metric	HLV+	HLVKI+	Voy+	ECC
GWTC-1 BBH Population—$\bar{R}_{\rm GWTC-1} = 24\ {\rm yr}^{-1}$				
$\langle\rho\rangle$	160	150	260	760
$\langle\Delta D_L/D_L\rangle$ (%)	3.2	2.3	1.5	0.43
ϵ^* (%)	4.3	24	43	91
Event rate ($\rm yr^{-1}$)	1.0	5.8	10	22
Heavy BBH Population—$\bar{R}_{\rm heavy} = 2.9\ {\rm yr}^{-1}$				
$\langle\rho\rangle$	250	250	460	1900
$\langle\Delta D_L/D_L\rangle$ (%)	1.9	1.3	0.79	0.17
ϵ^* (%)	9.6	48	76	100
Event rate ($\rm yr^{-1}$)	0.28	1.4	2.2	2.9
GW190814-like Population—$\bar{R}_{\rm GW190814-like} = 3.1\ {\rm yr}^{-1}$				
$\langle\rho\rangle$	63	75	160	530
$\langle\Delta D_L/D_L\rangle$ (%)	4.3	2.7	1.5	0.51
ϵ^* (%)	1.1	5.3	14	75
Event rate ($\rm yr^{-1}$)	0.034	0.16	0.43	2.3

Note. The medians are computed for the fraction ϵ^* of events in our simulation that satisfy the condition $\Omega_{90} \lesssim \Omega^* = 4.4 \times 10^{-2}\,{\rm deg}^2$, in the respective network. The table also lists the fraction ϵ^* and the corresponding number of events per year, for sources within a redshift of $z \leqslant 0.1$. The addition of two detectors in HLVKI+ compared to HLV+ improves the sky localization for all events, thus allowing quieter signals to fulfill $\Omega_{90} \lesssim \Omega^*$ and thus resulting in a decreased median S/N for the GWTC-1 population; see Figure 3 in the Appendix.

Equation (7) in Singer et al. 2016). Thus, from the full set of simulated events, we select the fraction ϵ^* that is resolved to $\Omega_{90} \lesssim \Omega^*$. This ensures a unique identification of the dark siren's host galaxy. Table 2 lists, for this subpopulation of events, medians of the S/N $\langle\rho\rangle$ and the fractional error in the luminosity distance $\langle\Delta D_L/D_L\rangle$. Furthermore, from the merger rate $\bar{R}$ and the fraction ϵ^*, we compute the number of well-localized dark sirens detected each year by the different networks. The listed event rates suggest that we can expect to observe one to several such events from the GWTC-1 and heavy BBH populations every 2 yr. GW190814-like binaries will be rarer at only one event every 25, 6.3, and 2.3 yr in HLV+, HLVKI+, and Voy+, respectively. The golden binaries described in Table 2 should all yield an error $\leqslant$5% in the luminosity distance, with the most accurate distance estimates to be expected from heavy binaries. Finally, the values in Table 2 clearly show that dark siren localization, both in terms of luminosity distance measurement and host galaxy identification, will be the norm in the 3G network era (ECC). In fact, the distance will be determined to subpercent accuracy no matter the source population.

7. Measurement of H_0 with Dark Sirens

The luminosity distance–redshift relation in the local universe is well approximated by the relation $D_L = cz/H_0$. It follows, then, that the fractional error in H_0 is equal to the fractional error in D_L for a single event, if errors in redshift measurements are negligible. One source of systematic error that affects the determination of H_0 is the selection bias that enters the analysis due to the consideration of only a subpopulation of actual events based on the events' sky localization. For the distances considered in this study, the selection bias reweights the H_0 posterior by a factor of $1/H_0^3$ (Chen et al. 2018). For the expected value of H_0 and the errors of interest in this study, the effect of this bias is to move the H_0 peak to lower values and widen the width of the posterior at the level of a percent for the worst errors quoted. In a Fisher study, only the errors in the estimation of a parameter are important and not the position of the peak of the posterior distribution. Consequently, we neglect the effects of the selections bias. In the left panel of Figure 2, we show the error in the measurement of H_0 by a single, golden event for each of the three dark siren subpopulations that obeys the localization condition $\Omega_{90} < \Omega^*$. We plot the median and variance of a distribution of H_0 errors for 100 realizations of a single random event drawn from each subpopulation. We find that HLV+, HLVKI+, and Voy+ detectors would estimate H_0 to a few percent accuracy, while the 3G network would measure H_0 to subpercent precision.

A major factor that contributes to the D_L errors is the D_L-ι degeneracy (Ajith & Bose 2009). This is most significant in the absence of strongly excited higher modes and, therefore, affects the nearly equal-mass binaries in the GWTC-1 and heavy BBH populations the most. It is precisely due to the importance of higher modes that golden GW190814-like events stay competitive to much higher-S/N signals from massive binaries. This holds especially true for less sensitive networks that are less effective at overcoming the D_L-ι degeneracy due to lower S/Ns. In fact, the variances in the distribution of H_0 errors do not favor any of the three dark siren populations in the 2G+ networks. It is not until the 3G era, when the heavy BBH events with high-S/Ns will yield significantly tighter bounds on H_0 than the GW190814-like ones.

Further, we note that the variance is larger for the GWTC-1 population compared to the heavy BBH and GW190814-like populations. This can be attributed to the wide mass distribution of the GWTC-1 population that ranges from $5\,M_\odot$ to $100\,M_\odot$: lower-mass binaries with relatively low S/N result in poorer luminosity distance measurements, but could still fulfill the sky localization condition. However, the GWTC-1 dark sirens stay competitive to the other two populations since they include both massive, high-S/N systems as well as very asymmetric ones.

In the right panel of Figure 2, we calculate the errors in H_0 by taking account of the number of detections (rounding to the nearest integer) in 2 yr of observing time for each network (assuming 100% duty cycle). The H_0 error estimates are missing for GW190814-like dark sirens in the case of HLV+ and HLVKI+, since we do not *expect* to observe *well-localized* dark sirens of either type in the respective networks within a 2 yr time period. We see that, due to the different rates of detections for different populations, the performance of the GW190814-like population is slightly worse (about a factor of 2) than the other two populations. Note also that the heavy BBH population is still competitive with the GWTC-1 BBHs even though its rate is considerably lower than the latter.

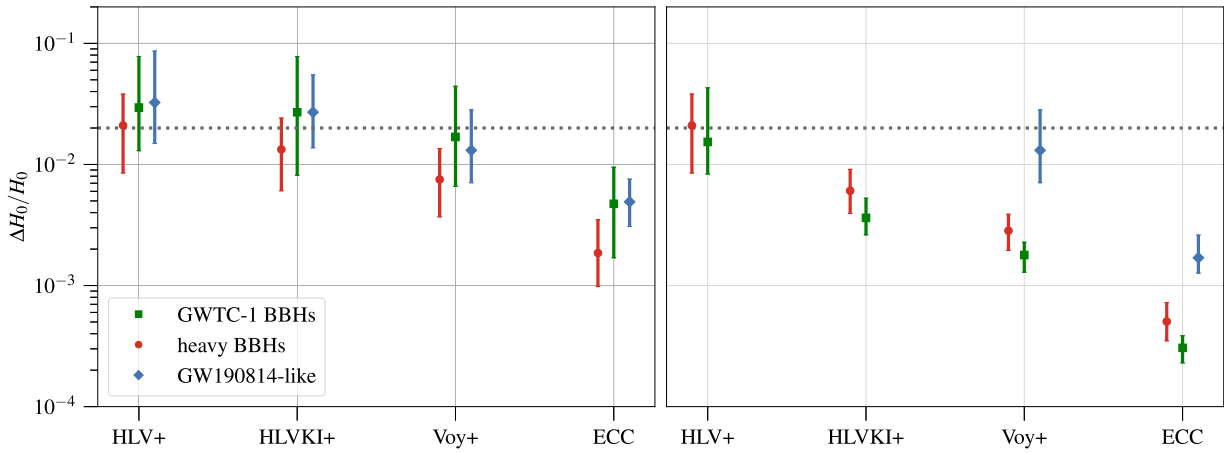

Figure 2. Left panel: the median and standard deviation of the distribution of fractional errors in H_0 measurement (assuming errors from redshift measurements are negligible) over 100 realizations for a single dark siren event for the four networks under study. All three populations we considered give statistically similar estimates of H_0. Right panel: same as the left panel, but the errors have been computed for the expected number of events in 2 yr of observing time for a network, assuming 100% duty cycle. The error estimates for some of the cases are not plotted because we do not expect to see any such event in an observing time of 2 yr.

8. Conclusions

We have demonstrated a tantalizing possibility of measuring the Hubble–Lemaître constant to ∼2% level precision using dark sirens with the imminent upgrades of the LIGO and Virgo detectors to 2G+ sensitivity. For highly asymmetric, low-mass systems like GW190814, the inclusion of higher spherical harmonic modes is crucial to make such a measurement especially in the A+ era, while heavier systems see less stark improvements; see the Appendix.

Our conclusions rely on controlling the amplitude calibration of the detectors to below $\lesssim$1%, which can be accomplished with photon calibrators (Karki et al. 2016), and two assumptions on a dark siren's host galaxy: its unique identification and a negligible uncertainty in peculiar velocity correction. The sky area could be "contaminated" with faint galaxies or the host itself could be faint and missing from current catalogs. Further, the host's peculiar velocity correction might not meet the desired accuracy, especially for nearby sources with small Hubble–Lemaître flow. Fortunately, EM follow-up observations of such well-localized sirens should be able to identify the host galaxy, obtain the redshift accurately by spectroscopy, model the velocity flow, and constrain the uncertainty in peculiar velocities to ∼100–150 km s^{-1} (Mukherjee et al. 2019), which is accurate enough for 99% of the sources considered in this study. Such follow-up surveys will be of interest to the entire astrophysics community since they would not only benefit from the Hubble–Lemaître constant measurement, but improve our understanding of the correlations between binary coalescences and their environments.

Given the paucity of binary neutron star mergers with EM counterparts so far, dark sirens offer an alternative to resolve the H_0 tension within the next 5 yr (LSC 2016). Beyond the 2G + era, our results are also very encouraging for a possible synergy between the dark sirens and the bright sirens, wherein the H_0 measurement from low redshift may be used as a prior in the measurement of other cosmological parameters at higher redshifts (Sathyaprakash et al. 2010).

We thank Archisman Ghosh, Leo Singer, and Salvatore Vitale for useful discussions and E. Hall and K. Kuns for providing Cosmic Explorer sensitivity curves. We thank Martin Hendry for carefully reading the manuscript and providing useful comments. B.S.S. is supported in part by NSF grant Nos. PHY-1836779, AST-1716394 and AST-1708146. S.B. and A. D. are supported by NSF grant No. PHY-1836779. K.G.A. is partially supported by a grant from the Infosys Foundation. K. G.A. acknowledges the Swarnajayanti grant DST/SJF/PSA-01/2017-18 DST-India and Core Research Grant EMR/2016/005594 of SERB. We thank all front line workers combating the CoVID-19 pandemic without whose support this work would not have been possible. This Letter has the LIGO document number LIGO-P2000229.

Appendix
Impact of Higher-mode Waveforms on Detectability, Sky Localization, and Distance Measurement

Figure 3 presents the cumulative density functions and medians of the 90% credible sky area Ω_{90}, S/N ρ, and fractional error in luminosity distance $\Delta D_L/D_L$ for the GWTC-1 BBH, heavy BBH, and GW190814-like populations, estimated with two different waveform models: one with higher modes, PhenomHM (London et al. 2018), and one without, PhenomD (Husa et al. 2016). We restricted the S/N and distance errors to the binaries in each population that fulfill the sky localization condition $\Omega_{90} < \Omega^* = 4.4 \times 10^{-2}\,\mathrm{deg}^2$ for either waveform. The graphs and quoted median values clearly illustrate the impact that waveforms with higher modes have on the systematics of a measurement: S/Ns are not affected in a meaningful way, but both sky localization and distance measurements show improvements. This holds especially true in the A+ era. The median 90% credible sky areas shrink by ∼20%–45% with higher-mode contributions, and the average distance errors improve by factors of ∼3–6. Even in a 3G network, we expect to observe an enhancement of the order ∼5%–25% in sky localization and ∼20%–45% for the distance measurement when including higher modes. Hence, these figures demonstrate the importance of the contribution of higher modes to achieve an accurate measurement of the sky location and luminosity distance, and consequently the Hubble constant.

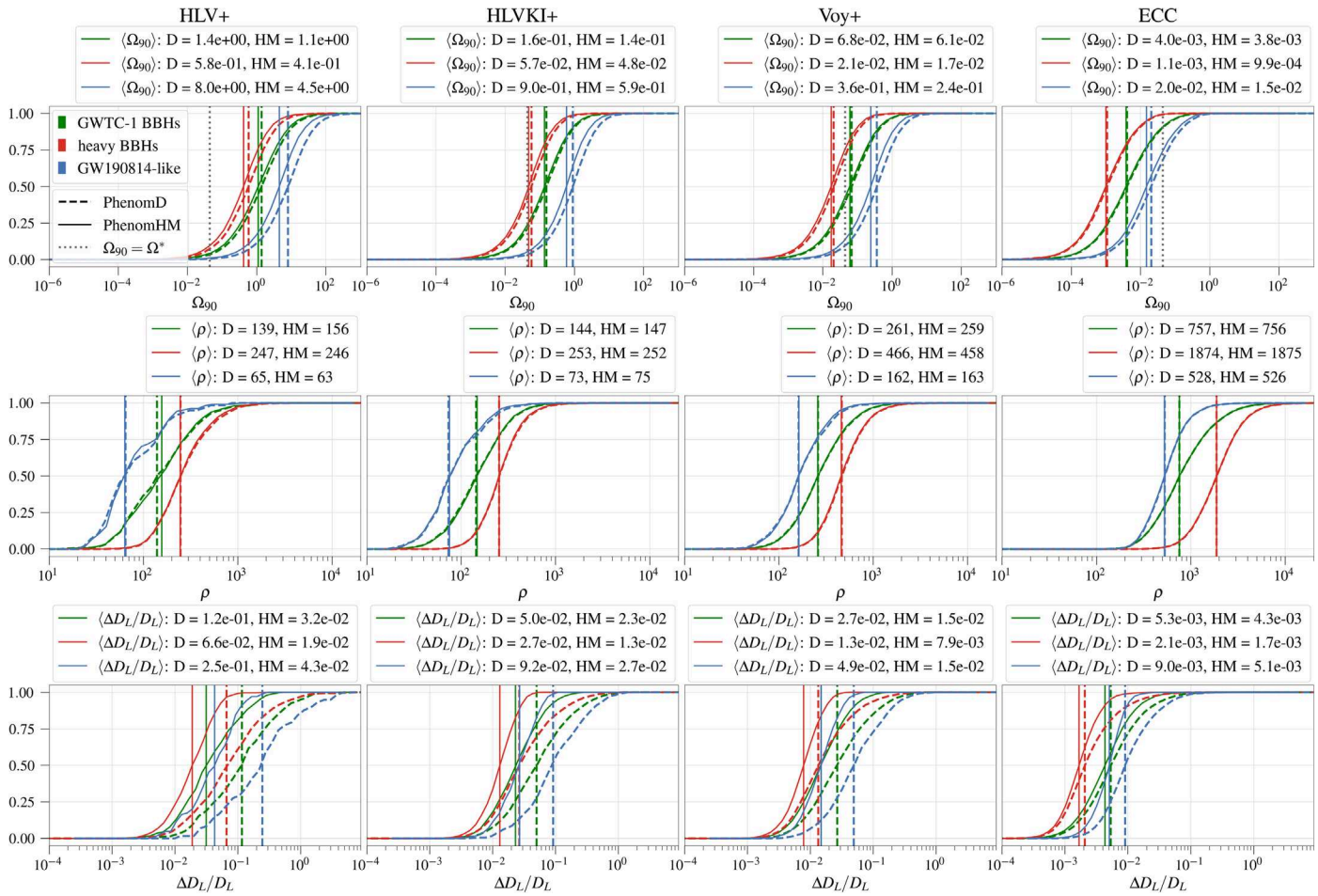

Figure 3. Cumulative density functions and medians of the 90% credible sky area Ω_{90}, S/N ρ, and fractional luminosity distance error $\Delta D_L/D_L$ calculated with two waveform models, one including higher modes (PhenomHM, solid) and the other without (PhenomD, dashed), for the GWTC-1 BBH, heavy BBH, and GW190814-like populations. S/Ns and distance errors are restricted to systems fulfilling $\Omega_{90} < \Omega^*$.

ORCID iDs

Ssohrab Borhanian https://orcid.org/0000-0003-0161-6109
Arnab Dhani https://orcid.org/0000-0001-9930-9101
Anuradha Gupta https://orcid.org/0000-0002-5441-9013
K. G. Arun https://orcid.org/0000-0002-6960-8538
B. S. Sathyaprakash https://orcid.org/0000-0003-3845-7586

References

Aasi, J., Abbott, B. P., Abbott, R., et al. 2015, CQGra, 32, 074001
Abbott, B. P., Abbott, R., Abbott, T. D., et al. 2017a, Natur, 551, 85
Abbott, B. P., Abbott, R., Abbott, T. D., et al. 2019c, PhRvX, 9, 031040
Abbott, B. P., Abbott, R., Abbott, T. D., et al. 2019a, arXiv:1908.06060
Abbott, B., Abbott, R., Abbott, T. D., et al. 2017b, PhRvL, 119, 161101
Abbott, B., Abbott, R., Abbott, T. D., et al. 2018a, LRR, 21, 3
Abbott, B., Abbott, R., Abbott, T. D., et al. 2019b, ApJL, 882, L24
Abbott, R., Abbott, T. D., Abraham, S., et al. 2020a, PhRvD, 102, 043015
Abbott, R., Abbott, T. D., Abraham, S., et al. 2020b, ApJL, 896, L44
Abbott, T. M. C., Abdalla, F. B., Allam, S., et al. 2018b, ApJS, 239, 18
Acernese, F., Agathos, M., Agatsuma, K., et al. 2015, CQGra, 32, 024001
Ade, P., Aghanim, N., Arnaud, M., et al. 2016, A&A, 594, A13
Adhikari, R., Arai, K., Brooks, A. F., et al. 2020, CQGra, 37, 165003
Aghanim, N., Akrami, Y., Ashdown, M., et al. 2020, A&A, 641, A6
Ajith, P., & Bose, S. 2009, PhRvD, 79, 084032
Akutsu, T., Ando, M., Arai, K., et al. 2019, NatAs, 3, 35
Arun, K. G., Iyer, B. R., Sathyaprakash, B. S., Sinha, S., & Van Den Broeck, C. 2007, PhRvD, 76, 104016
Bahcall, N. A. 1995, arXiv:astro-ph/9611148
Calderón Bustillo, J., Dietrich, T., & Lasky, P. D. 2020, arXiv:2006.11525
Chen, H.-Y., Fishbach, M., & Holz, D. E. 2018, Natur, 562, 545
Cutler, C., & Flanagan, E. 1994, PhRvD, 49, 2658
Dálya, G., Galgóczi, G., Dobos, L., et al. 2018, MNRAS, 479, 2374
Drlica-Wagner, A., Sevilla-Noarbe, I., Rykoff, E. S., et al. 2018, ApJS, 235, 33
Freedman, W. L., Madore, B. F., Hatt, D., et al. 2019, ApJ, 882, 34
Graff, P. B., Buonanno, A., & Sathyaprakash, B. S. 2015, PhRvD, 92, 022002
Gray, R., Hernandez, I. M., Qi, H., et al. 2020, PhRvD, 101, 122001
Holz, D. E., & Hughes, S. A. 2005, ApJ, 629, 15
Howell, E., Chan, M. L., Chu, Q., et al. 2018, MNRAS, 474, 4385
Husa, S., Khan, S., Hannam, M., et al. 2016, PhRvD, 93, 044006
Kalaghatgi, C., Hannam, M., & Raymond, V. 2020, PhRvD, 101, 103004
Karki, S., Tuyenbayev, D., Kandhasamy, S., et al. 2016, RScI, 87, 114503
Kuns, K., Srivastava, V., Hall, E., Evans, M., & Ballmer, S. 2020a, Cosmic Explorer Technical Document, https://dcc.cosmicexplorer.org/CE-T2000007
Kuns, K. A., Yu, H., Chen, Y., & Adhikari, R. X. 2020b, PhRvD, 102, 043001
LIGO Scientific Collaboration 2018, LIGO Algorithm Library—LALSuite, Free Software (GPL), https://git.ligo.org/lscsoft/lalsuite
London, L., Khan, S., Fauchon-Jones, E., et al. 2018, PhRvL, 120, 161102
LSC 2016, LSC Technical Document, https://dcc.ligo.org/LIGO-T1600119/public
Mukherjee, S., Lavaux, G., Bouchet, F. R., et al. 2019, arXiv:1909.08627
Nishizawa, A. 2017, PhRvD, 96, 101303
Punturo, M., Abernathy, M., Acernese, F., et al. 2010, CQGra, 27, 084007
Reitze, D., Adhikari, R. X., Ballmer, S., et al. 2019, BAAS, 51, 35
Riess, A. G., Casertano, S., Yuan, W., Macri, L. M., & Scolnic, D. 2019, ApJ, 876, 85
Roy, S., Sengupta, A. S., & Arun, K. 2019, arXiv:1910.04565
Sathyaprakash, B. S., Schutz, B. F., & Van Den Broeck, C. 2010, CQGra, 27, 215006
Schutz, B. F. 1986, Natur, 323, 310

SDSS 2016, GWENS Catalogue, https://astro.ru.nl/catalogs/sdss_gwgalcat/
Singer, L. P., Chen, H.-Y., Holz, D. E., et al. 2016, ApJL, 829, L15
Van Den Broeck, C., & Sengupta, A. S. 2007, CQGra, 24, 1089
Verde, L., Treu, T., & Riess, A. 2019, NatAs, 3, 891
Wong, K. C., Suyu, S. H., Chen, G. C.-F., et al. 2020, MNRAS, 498, 1420
Yu, J., Wang, Y., Zhao, W., & Lu, Y. 2020, arXiv:2003.06586